Stochastic and superharmonic stochastic resonances of a confined overdamped harmonic oscillator

Lu Zhang,[1,*] Li Lai,[1] Hao Peng,[2] Zhe Tu,[3] and Suchuan Zhong[4,5,†]
[1]*College of Mathematics, Sichuan University, Chengdu, 610065, China*
[2]*College of Mathematics, Southwest Jiaotong University, Chengdu, 611756, China*
[3]*Business School, Zhejiang Wanli University, Ningbo, 315100, China*
[4]*School of Aeronautics and Astronautics, Sichuan University, Chengdu, 610065, China*
[5]*BBD Inc, Chengdu, 610093, China*

(Received 9 March 2017; revised manuscript received 30 October 2017; published 29 January 2018)

The dynamics of many soft condensed matter and biological systems is affected by space limitations, which produce some peculiar effects on the systems' stochastic resonance (SR) behavior. In this study, we propose a model where SR can be observed: a confined overdamped harmonic oscillator that is subjected to a sinusoidal driving force and is under the influence of a multiplicative white noise. The output response of the system is a periodic signal with harmonic frequencies that are odd multiples of the driving frequency. We verify the amplitude resonances at the driving frequencies and superharmonic frequencies that are equal to three, five, and seven times the driving frequency, using a numerical method based on the stochastic Taylor expansion. The synergistic effect of the multiplicative white noise, constant boundaries, and periodic driving force that can induce a SR in the output amplitude at the driving and superharmonic frequencies is found. The SR phenomenon found in this paper is sensitive to the driving amplitude and frequency, inherent potential parameter, and boundary width, thus leading to various resonance conditions. Therefore, the mechanism found could be beneficial for the characterization of these confined systems and could constitute an important tool for controlling their basic properties.

DOI: 10.1103/PhysRevE.97.012147

I. INTRODUCTION

Stochastic resonance (SR) is an interesting phenomenon typically found in nonlinear dynamic systems driven by a periodic force and noise [1–3]. The SR-like phenomenon has gained extensive attention because of its significant practical applications. Numerous early studies mainly focus on the phenomenon of SR occurring in nonlinear equations. However, later researchers found that multiplicative SR in linear systems is a general phenomenon [4–8]. Afterwards, SR was also found in the excitable systems [9] and nondynamical systems without response thresholds [10]; the input external signal can be either a weak periodic signal or a chaotic signal [11]; the added noise can be either additive noise or multiplicative noise [6]. The phenomenon of stochastic multiresonances [12,13] was also found, that is, with the change in noise intensity, the resonance peak appears at the multiple noise intensities. The studies on complex neuronal networks in Refs. [12,13] have shown that appropriately tuned delays can also induce the system to produce stochastic multiresonances.

Most studies on SR have focused on models without boundaries. However, when scaling down the size of a system, in situations frequently found in soft condensed matter and biological systems, particles move in constrained regions with boundaries such as small cavities, pores, or channels [14–16]. The dynamics of these systems will be affected by the space limitations, which exert unique effects on the reaction, diffusion, and SR behavior of the systems. A system with boundaries is no longer an open system but a local system, and uneven boundaries usually have the effect of entropic barriers [16–19]. In 2002, Schüring [20] *et al.* studied the influence of the entropic potential on the diffusion of zeolite in molecular dynamics. In 2003, Schweizer *et al.* [21] studied the entropic potential of colloidal suspensions and discussed particle transport in microscopic dynamics. Reguera *et al.* [22] found that the entropic potential caused by uneven boundaries could effectively control particle transport in a quasi-one-dimensional structure.

Burada [23] introduced the entropic potential in irregularly shaped media in two-dimensional space and found a noise-induced resonantlike behavior known as the entropic stochastic resonance (ESR). However, previous studies on ESR have primarily focused on Brownian particle movement in two-dimensional space [23–26]. Gravity in the vertical direction and uneven boundaries are crucial for the ESR to experience the entropic barrier. Very recently, SR has also been found even in the absence of an energetic or an entropic barrier while in the presence of a geometric confinement, which is known as geometric stochastic resonance (GSR) [27]. To our knowledge, the response and SR of Brownian particle movement in a one-dimensional space restricted by constant boundaries are rarely reported.

Alternatively, in the case of one-dimensional discrete-time systems, SR-like behavior analogous to ESR and GSR can be observed in one-dimensional chaotic maps subjected to sinusoidal multiplicative periodic forcing, where the output trajectory is restricted to one of two subintervals and the inherent chaos of the system could act as noise [28,29]. Moreover, we can reasonably assume that similar SR-like

*zhanglumail@gmail.com
†Corresponding author: zsczsc48@hotmail.com

behavior occurs in a continuous-time system described by differential equations.

In this study, given that a Brownian particle is subjected to a sinusoidal driving force and another varying force caused by the presence of a random fluctuating monostable potential, its original motion equation is a linear Langevin equation driven by multiplicative white Gaussian noise. In Ref. [5], Berdichevsky and Gitterman found that for the linear Langevin equation, SR occurs only for color multiplicative noise and is absent for white multiplicative noise. However, the restricted boundaries considered in this study actually produce nonlinearity in the dynamics of the original linear system: the average output amplitude A_Ω at the driving frequency Ω is a nonmonotonic function of noise intensity D; that is, classical SR was found. Therefore, for our system, gravity and geometric unevenness are not essential for the occurrence of SR in a confined space. Even if the system is only affected by multiplicative white noise, the confinement of the particle is crucial for SR. The occurrence of SR proposed in this paper depends on the width of the boundaries, system parameters, and can then be controlled by them. Thus, understanding the role of noise and space confinement in this paper does provide application of a periodic driving force result in a spectral amplification at an optimum value of the ambient noise level.

Moreover, most of the previous studies on SR focus on the response at the frequency of the driving force. Several recent studies on nonlinear systems also found that noise can induce a resonance at high-order harmonics that are odd multiples of the driving frequency [30–34]. In this study, the presence of boundaries was also found to lead to high-order harmonics in the output response. The results show that the multiplicative white noise can not only induce an amplitude resonance at the driving frequency, but also at the superharmonic frequencies that are odd multiples of the driving frequency.

The rest of the study is organized as follows. In Sec. II, we introduce the considered system and then present a numerical Brownian dynamics algorithm based on the stochastic Taylor expansion (STE) to calculate the average output amplitude of the considered system. In Sec. III, we first check the validity of the presented STE-based Brownian dynamics algorithm and then investigate the noise-induced SR at the driving and superharmonic frequencies. Finally, the results are discussed and the main conclusions are drawn in Sec. IV.

II. MODEL AND METHOD

In this study, a Brownian particle moving in a confined one-dimensional space is considered. The particle is subjected to a periodic sinusoidal driving force and another varying force caused by a random fluctuating monostable potential. The overdamped dynamics which neglects inertial effects can be described by the following linear Langevin equation:

$$\dot{x} = -[a + \xi(t)]x + A\sin(\Omega t), \tag{1}$$

where t is the time, and x is the position of the particle along the x axis. $A > 0$ and $\Omega > 0$ are the amplitude and angular frequency of the periodic driving force, respectively. The potential parameter a describes the decay rate of the output response to the equilibrium point in the absence of noise. $\xi(t)$ represents a standard Gaussian white noise with a vanishing mean and noise intensity D satisfying $\langle\xi(t)\rangle = 0$ and $\langle\xi(t)\xi(s)\rangle = 2D\delta(t-s)$. Equation (1) has many applications, such as problems of fluctuating barrier crossing in chemistry, enzymatic kinetics in biology, and nuclear magnetic resonance in physics [5].

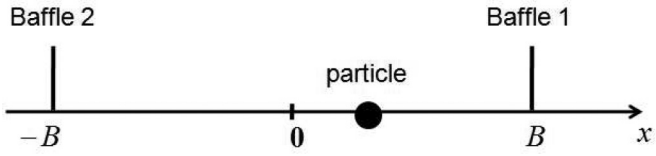

FIG. 1. Schematic diagram of the 1D structure, where the Brownian particle moves in the confined interval. The x-axis coordinates of the two vertical baffles are correspondingly $x = -B$ and B, where B is the half-width of the boundary.

When scaling down the size of systems, the particles in these systems are always confined to move in a constrained space. In this study, the movement of the particle is supposed to be confined by two vertical baffles (i.e., boundaries). For the geometry shown in Fig. 1, the dynamics of Eq. (1) can be considered as the reflecting boundary conditions. When the Brownian particle meets one of the boundaries, the particle will be vertically rebounded and then return between the two boundaries.

A. In the absence of restricted boundaries

In the absence of restricted boundaries, the exact average solution of Eq. (1) is given by [5]

$$\langle x(t)\rangle = x(0)\langle e^{-\int_0^t \xi(s)ds}\rangle e^{-at} + Ae^{-at}\int_0^t \sin(\Omega u)e^{au}\langle e^{-\int_0^{t-u}\xi(s)ds}\rangle du, \tag{2}$$

where $\langle\ldots\rangle$ denotes an ensemble average over the distribution of the random forces.

Suppose $B(t)$ is a standard Brown motion, satisfies $B(t) \sim N(0,t)$, and then for the Gaussian white noise $\xi(t)$, $-\int_0^t \xi(s)ds$ is a Brownian motion with drift, which has a zero drift coefficient, and a diffusion coefficient of $2D$, i.e., $-\int_0^t \xi(s)ds \sim N(0,2Dt)$. Moreover, $e^{-\int_0^t \xi(s)ds}$ is a geometric Brown motion, and thus we have [35]

$$\langle e^{-\int_0^t \xi(s)ds}\rangle = e^{Dt},\ \langle e^{-\int_0^{t-u}\xi(s)ds}\rangle = e^{D(t-u)}. \tag{3}$$

Substituting Eq. (3) into (2) we have

$$\langle x(t)\rangle = x(0)e^{-(a-D)t} + Ae^{-(a-D)t}\int_0^t \sin(\Omega u)e^{(a-D)u}du. \tag{4}$$

Here, the integra $\int_0^t \sin(\Omega u)e^{(a-D)u}du$ in Eq. (4) can be obtained by partial integral method:

$$\int_0^t \sin(\Omega u)e^{(a-D)u}du = \frac{\Omega}{(a-D)^2+\Omega^2} + \frac{1}{\sqrt{(a-D)^2+\Omega^2}}\cos(\Omega t+\Theta)e^{(a-D)t}, \tag{5}$$

in which $\Theta = \arctan(\frac{a-D}{\Omega}) + \pi$.

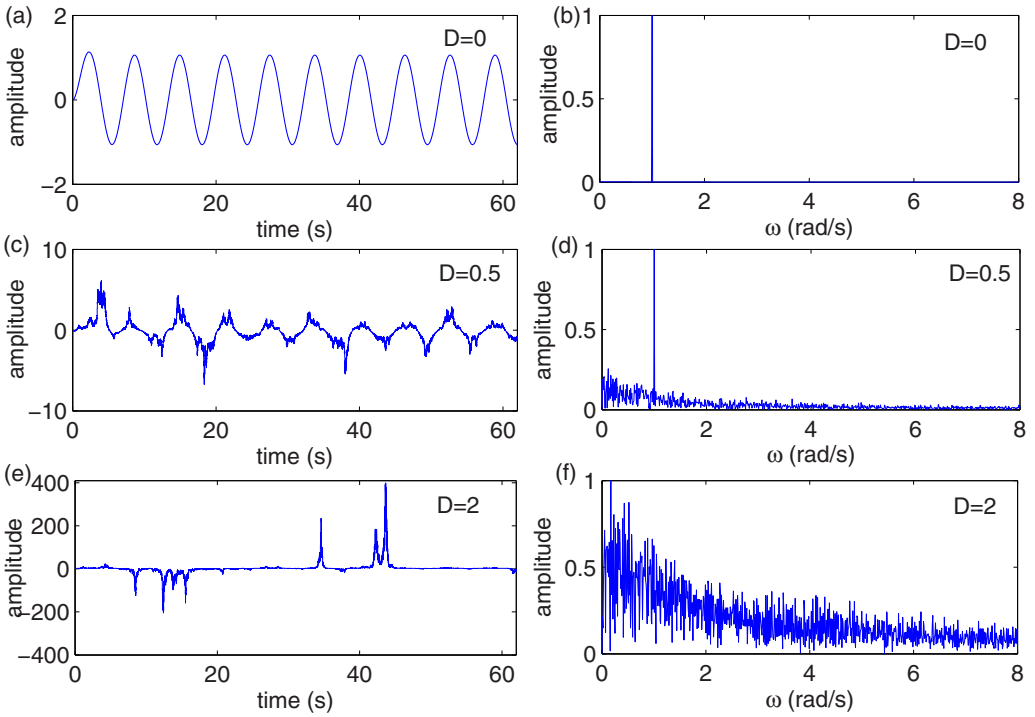

FIG. 2. Trajectories and normalized frequency spectrums of the output responses of the Brownian particle in the absence of boundaries at $A = 1.5$, $\Omega = 1$, $a = 1$ with different values of D: (a), (b) $D = 0$; (c), (d) $D = 0.5$; (e), (f) $D = 2$. When $D = 0$ [as shown in (b)], the output response is a single frequency signal; when $D < a = 1$ [as shown in (a) and (c)], the average position $\langle x(t)\rangle$ is bounded; while $D > a = 1$ [as shown in (e)], the average position $\langle x(t)\rangle$ is unbounded.

Substituting Eq. (5) into (4) we have the average solution of Eq. (1):

$$\langle x(t)\rangle = Ce^{-(a-D)t} + A_{st}\cos(\Omega t + \Theta), \tag{6}$$

in which

$$C = x(0) + \frac{A\Omega}{\Omega^2 + (a-D)^2},\ A_{st} = \frac{A}{\sqrt{\Omega^2 + (a-D)^2}},$$
$$\Theta = \arctan\left(\frac{a-D}{\Omega}\right) + \pi. \tag{7}$$

For the noise intensity $D < a$, the exponent decay term $Ce^{-(a-D)t}$ will tend to zero in the long time limit $t \to +\infty$, which yields the average position $\langle x(t)\rangle$ bounded. Thus, in this case, the stationary solution of Eq. (1) in the asymptotic time limit (i.e., after the memory of the initial conditions is completely lost) is

$$\langle x(t)\rangle_{st} = A_{st}\cos(\Omega t + \Theta), \tag{8}$$

whose amplitude A_{st} is a monotonic function of D, that is, there is no SR for this linear system with multiplicative white noise in the absence of boundaries. This result is not surprising because the white noise has no characteristic frequency which would be "in resonance" with an external frequency. Recall that in the nonlinear case such a characteristic frequency can be constructed for a random force (the Kramers rate) [5]. Moreover, note that for all $D > a$, the exponent term $Ce^{-(a-D)t}$ will be infinite as $t \to +\infty$, so that $\langle x(t)\rangle$ is unbounded in the absence of boundaries. For different values of the noise intensity D, Fig. 2 presents three trajectories and three normalized frequency spectrums of the output responses of the linear Langevin equation (1) in the absence of restricted boundaries. However, it can be seen from the following discussions the addition of the boundaries makes the exponent term $Ce^{-(a-D)t}$ bounded, thus resulting in changes in the dynamics properties of the particle.

B. In the presence of restricted boundaries

In the presence of restricted boundaries, if the boundary half-width satisfies $B \leqslant A_{st}$, and A_{st} is given in Eq. (7), then the boundaries will have a bounding effect on the Brownian particle. Therefore, the Brownian particle undergoes a constrained motion. When the particle moves near one of the baffles, the particle would meet the boundary via the effects of the external potential field and periodic driving force. Subsequently, the particle rebounds back from the boundary. However, the effects of the external potential field and periodic force are continuous. Thus, the particle will quickly return to meet the boundary and repeatedly rebound until the particle moves away from the boundary under the effects of the external potential field and the periodic force. Afterwards, the particle will move close to another boundary, and then the same process will be repeated.

However, no generally valid analytical expressions are possible in the presence of restricted boundaries. The behavior of the particle of interest can be simulated using the standard stochastic Euler algorithm, which requires a small integration step time and high computation time. Thus, in this study, a numerical method based on STE is adopted to simulate the Langevin equation (1) [36,37]. After calculation, we obtained the numerical formula (9) as follows, whose derivation is

illustrated in the Appendix:

$$\begin{aligned} x(t+h)-x(t) &= \left[-ah+\tfrac{1}{2}a^2h^2\right]x(t)-\tfrac{1}{2}ah^2A\sin(\Omega t) \\ &\quad -\frac{A}{\Omega}\{\cos[\Omega(t+h)]-\cos(\Omega t)\} \\ &\quad +\left((ah-1)\Gamma_1(t+h)+\tfrac{1}{2}[\Gamma_1(t+h)]^2\right)x(t) \\ &\quad -[h\Gamma_1(t+h)-\Gamma_2(t+h)]A\sin(\Omega t), \end{aligned} \tag{9}$$

wherein h is the integration step time, random variables $\Gamma_1(t+h)$ and $\Gamma_2(t+h)$ are given by Eq. (A17).

Therefore, suppose the position of $x(t)$ at $t=nh$ is $x[n]$ and $\Gamma_1[n+1]=\Gamma_1(t+h)$ and $\Gamma_2[n+1]=\Gamma_2(t+h)$, then the single integration steps read as

$$\begin{aligned} x[n+1] &= \left(1-ah+\tfrac{1}{2}a^2h^2\right)x[n]-\tfrac{1}{2}ah^2A\sin(\Omega nh) \\ &\quad -\frac{A}{\Omega}\{\cos[\Omega(n+1)h]-\cos(\Omega nh)\} \\ &\quad +\left[a\Gamma_2[n+1]-\Gamma_1[n+1]+ah\Gamma_1[n+1]\right. \\ &\quad \left.-a\Gamma_2[n+1]+\tfrac{1}{2}(\Gamma_1[n+1])^2\right]x[n] \\ &\quad -[h\Gamma_1[n+1]-\Gamma_2[n+1]]A\sin(\Omega nh). \end{aligned} \tag{10}$$

Second, we consider the case when the particle is confined in the interval $[-B,B]$:

(i) If $|x[n+1]|\leqslant B$, the modification position is as follows:

$$\tilde{x}[n+1]=x[n+1], \tag{11}$$

where $x[n+1]$ is the original position and is given by Eq. (10), and $\tilde{x}[n+1]$ is the new position.

(ii) If $x[n+1]>B$, and the velocity is $v[n]=(x[n+1]-x[n])/h$, the particle will meet one of the boundaries. In this case, a simple process, such as specular reflection, is used to simulate the movement of particle near the boundary. When the particle meets the boundary, the particle is vertically rebounded with the same magnitude of the velocity and the reversed direction of motion, and the time step is incremented as follows:

$$\begin{aligned} \tilde{x}[n+1] &= B-v[n]\left(h-\frac{B-x[n]}{v[n]}\right) \\ &= 2B-x[n+1]. \end{aligned} \tag{12}$$

(iii) If $x[n+1]<-B$, similarly, the time step is incremented as follows:

$$\begin{aligned} \tilde{x}[n+1] &= -B-v[n]\left(h-\frac{-B-x[n]}{v[n]}\right) \\ &= -2B-x[n+1]. \end{aligned} \tag{13}$$

For different values of the noise intensity D, Fig. 3 presents three trajectories and normalized frequency spectra of the steady-state responses of the confined Langevin equation (1) in the presence of boundaries. Here, the "baffles," which confine the trajectory to a finite domain are highly similar to the folding operation of the map given in Refs. [28,29]. In Refs. [28,29], the SR-like behavior of the chaotic map was observed. The system with restricted boundaries is analogous to the classical bistable well scenario of SR. In the presence of the boundaries, the output trajectory of the system is restricted to either of the two subintervals. The subintervals correspond to the two wells between which the system hops to and fro, aided by the inherent white noise and the periodic signal.

As shown in Fig. 3(a), because of the effect of the boundaries, the output steady-state response can be regarded as a sinusoidal signal confined by a rectangle envelope. Such a signal has high-order harmonics that are odd multiples of the driving frequency. Thus, the frequency components in the frequency spectra of the steady-state responses [as shown in Figs. 3(b), 3(d), and 3(f)] not only contain the driving angular frequency Ω, but also has superharmonic frequencies, namely, $3\Omega,5\Omega,7\Omega,\ldots$, which are odd multiples of the driving angular frequency. Interestingly, the amplitude of the frequency components at superharmonic frequencies (e.g., $\omega=3\Omega,5\Omega,7\Omega$) becomes more evident as D increases. Thus, for this considered linear system (1) in the presence of boundaries, the periodic signal and noise cannot cooperate within the framework of linear dynamics, such that energy transformation from the noise to the signal may exist.

III. STOCHASTIC AND SUPERHARMONIC STOCHASTIC RESONANCES IN A CONFINED ONE-DIMENSIONAL SPACE

As seen from the above discussion, the response of the system in Eq. (1) in the absence of restricted boundaries to the periodic input signal $F(t)=A\sin(\Omega t)$ is a periodic function of time. The average value of the position $x(t)$ in the asymptotic time limit of the confined Langevin equation can be written in the following Fourier series form:

$$\langle x(t)\rangle_{st}=\sum_{k=0}^{+\infty}A_{(2k+1)\Omega}\cos[(2k+1)\Omega t-\Phi_{(2k+1)\Omega}], \tag{14}$$

where $A_{k\Omega}$ and $\Phi_{k\Omega}$ are the average response amplitude and phase lag at the angular frequency $k\Omega$, respectively. These quantities are obtained by averaging the inhomogeneous process $x(t)$ over the ensemble of different random path realizations. In particular, the average particle position of Eq. (1) is

$$\langle x(t)\rangle=\frac{1}{K}\sum_{i=1}^{K}x_i(t), \tag{15}$$

where $x_i(t)$ is the system output response of the ith Monte Carlo simulation, $i=1,2,\ldots,K$.

Therefore, the response amplitude and the phase lag at the angular frequency $k\Omega$ are computed by

$$A_{k\Omega}=\sqrt{Q_{\sin}^2+Q_{\cos}^2}, \tag{16}$$

$$\Phi_{k\Omega}=\arctan(Q_{\sin}/Q_{\cos}), \tag{17}$$

where $Q_{\sin}$ and $Q_{\cos}$ are the sine and cosine components of the Fourier transform, specifically,

$$\begin{aligned} Q_{\sin} &= \frac{2}{NT_0}\int_0^{NT_0}\langle x(t)\rangle\sin(k\Omega t)dt, \\ Q_{\cos} &= \frac{2}{NT_0}\int_0^{NT_0}\langle x(t)\rangle\cos(k\Omega t)dt, \end{aligned} \tag{18}$$

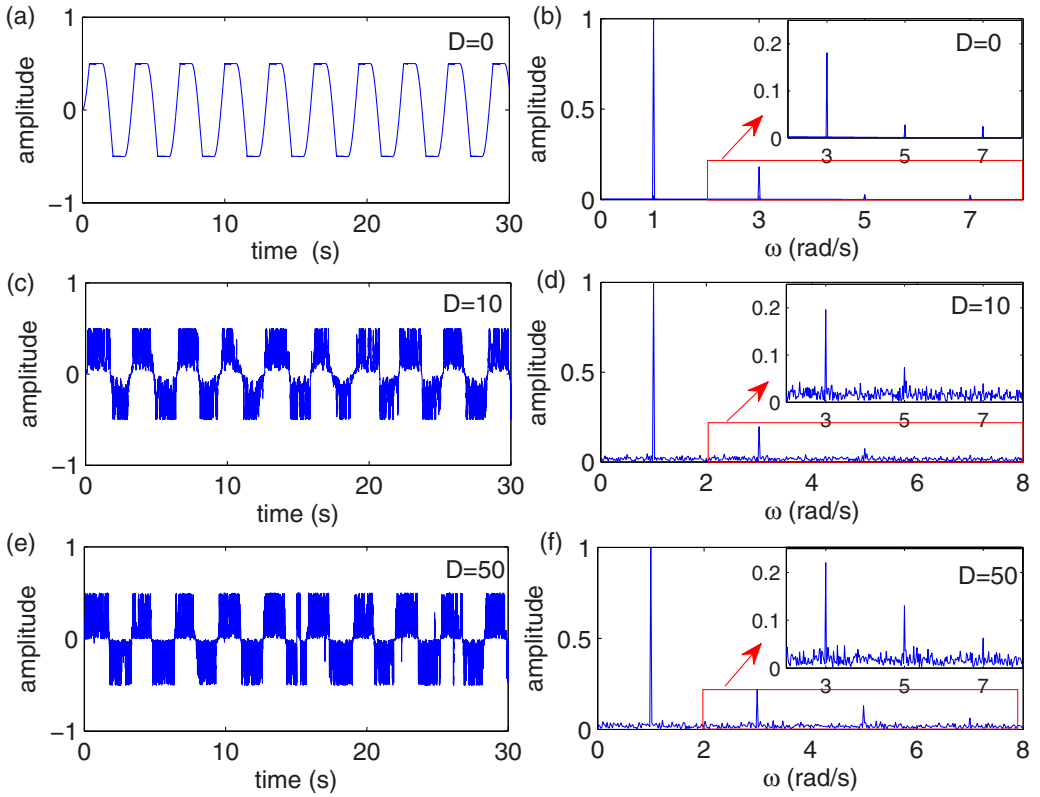

FIG. 3. Trajectories and normalized frequency spectrums of the output response of the Brownian particle confined by boundary in Fig. 1 at $B = 0.5$, $A = 1.5$, $\Omega = 1$, $a = 1$ with different values of D: (a), (b) $D = 0$; (c), (d) $D = 10$; (e), (f) $D = 50$. In the absence of white noise ($D = 0$), the particle regularly dwells between the two boundaries. The regularity of the particle decreases with the increase in noise intensity D.

where $T_0 = 2\pi/\Omega$ and N is the period number, which is a large integer, indicating that the effect of the initial condition on the response can be ignored.

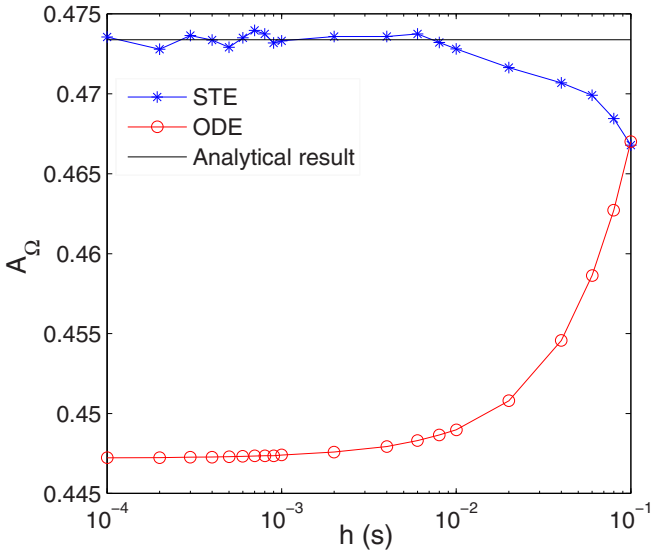

FIG. 4. Comparison of average amplitude A_Ω as a function of the time step h, obtained by ODE, the present STE and the analytical result in the absence of boundaries, in which, $a = 1$, $\Omega = 2$, $D = 0.32$, and $N = 100$.

In previous references of SR, in Eq. (16), k is always chosen as $k = 1$. However, in the proposed case, the superharmonics with high-order odd frequencies induced by the boundary also exist. Therefore, in this study, we will consider the SR of the Ω harmonic and the SR of the higher-order harmonics. The high-order harmonic angular frequencies 3Ω, 5Ω, and 7Ω were selected in the following analysis to simplify the problem. The average amplitude at the driving angular frequency Ω was chosen for comparison.

A. Validity of the present Brownian dynamics algorithm

To determine the validity of the present STE-based Brownian dynamics algorithm, the present results should be compared with the analytical results given by Eq. (7) in the absence of boundaries. In the absence of boundaries, Eqs. (16) and (18) are used to calculate the average response amplitude A_Ω at the angular frequency Ω obtained by the present STE algorithm and ordinary differential equation (ODE) algorithm as a function of the time step h in Fig. 4. The results from the present STE-based algorithm agree well with that from the analytical results for the small time step. Moreover, the accuracy of the present algorithm is higher than that of the ODE algorithm.

The convergence of the STE-based algorithm in the presence of boundaries was verified. Figure 5 illustrates that the STE algorithm is convergent. Figure 5(a) illustrates that the numerical results do not depend on the time step h for $h \leqslant 0.001$, Fig. 5(b) shows that the numerical results do not depend

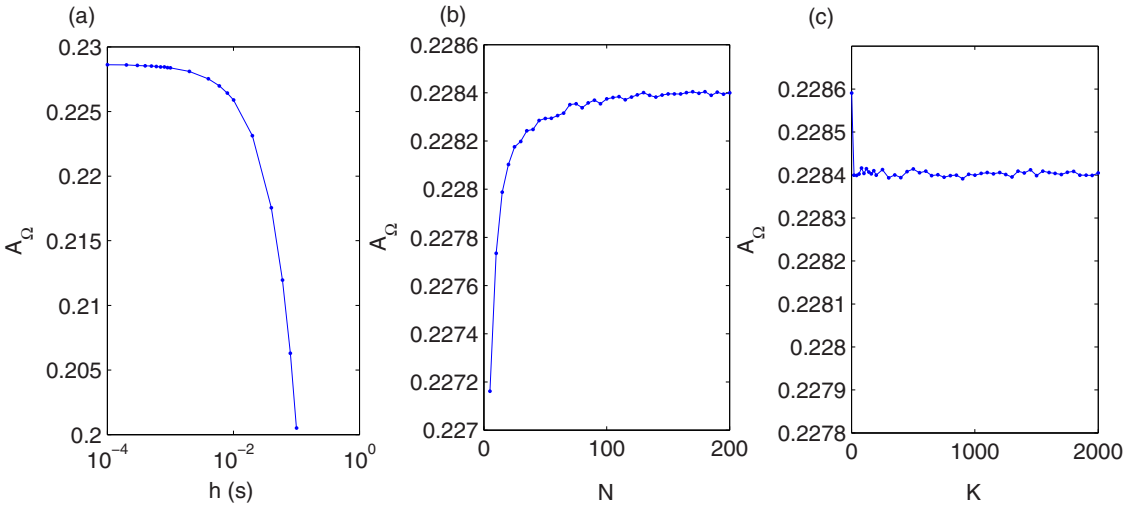

FIG. 5. Average A_Ω obtained by the present STE in the presence of boundaries: (a) the average A_Ω obtained by the present STE algorithm as a function of h with $B = 0.2, a = 1, \Omega = 2, D = 0.08, N = 100$, and $K = 1000$; (b) the average A_Ω obtained by the present STE algorithm as a function of N with $B = 0.2, a = 1, \Omega = 2, D = 0.08, K = 1000, h = 0.001$s; (c) the average A_Ω obtained by the present STE algorithm as a function of K with $B = 0.2, a = 1, \Omega = 2, D = 0.08, N = 100$, and $h = 0.001$ s.

on K for $K \geqslant 1000$. Figure 5(c) shows that the numerical results do not depend on K for $K \geqslant 1000$. Therefore, to provide the requested accuracy, the time step was chosen to be $h = 0.001$ s, the period number N was set to 100, and the average particle position $\langle x(t) \rangle$ along the x direction was derived from an ensemble average of approximately $K = 1000$ trajectories according to the expression (15).

B. Stochastic and superharmonic stochastic resonances

To study the SR appearance, the average amplitude $A_{k\Omega}$ at frequency $k\Omega$ with $k = 1,3,5,7$ was analyzed in the presence of boundaries, which are defined by Eq. (16). Extensive numerical simulations based on Eqs. (10)–(13) and Eqs. (16)–(18) were performed to determine the average output amplitude.

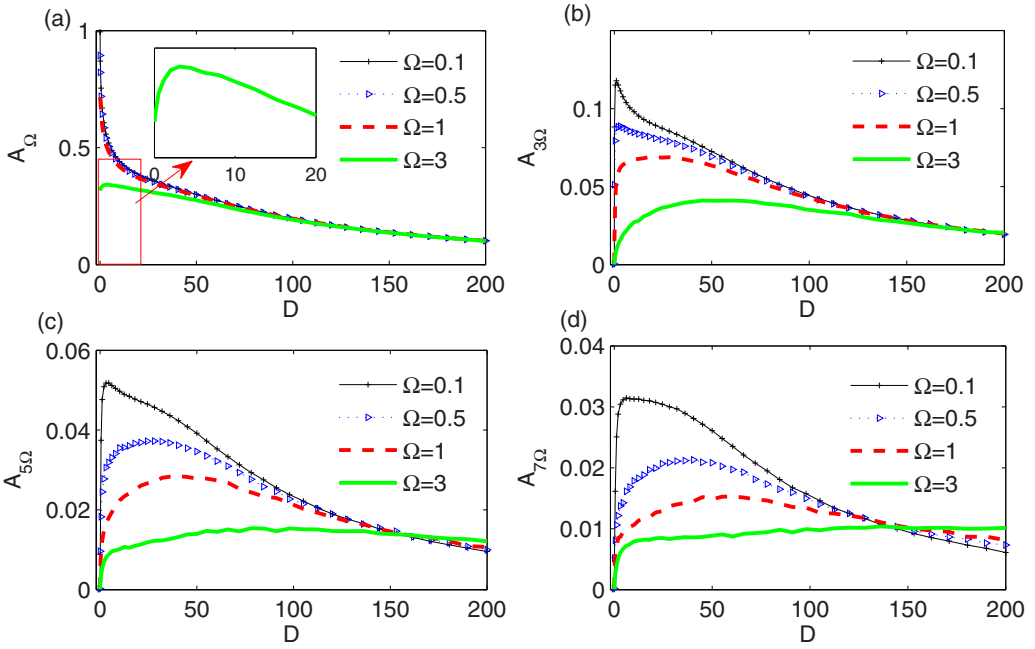

FIG. 6. Average response amplitude $A_{k\Omega}, k = 1,3,5,7$, versus the noise intensity D for different values of the driving angular frequency Ω, in which $A = 1$, $a = 1$, $B = 1$. For small angular frequency Ω, e.g., $\Omega = 0.1$, 0.5, and 1, the average response amplitude A_Ω is a decreasing function of D, and no SR exists; $A_{k\Omega}$ ($k = 3,5,7$) shows the nonmonotonicity with D, that is, the SRs at the superharmonics that are odd multiples of the basic driving frequency occur, which we called as superharmonic SR. For large values of Ω, e.g., $\Omega = 3$, the SR exists in all the $A_{k\Omega} - D$ curves ($k = 1,3,5,7$). Moreover, the interwell dynamics responsible of the appearance of the main peak in $A_{k\Omega}$ at higher noise intensities is not remarkably affected by the driving frequency Ω.

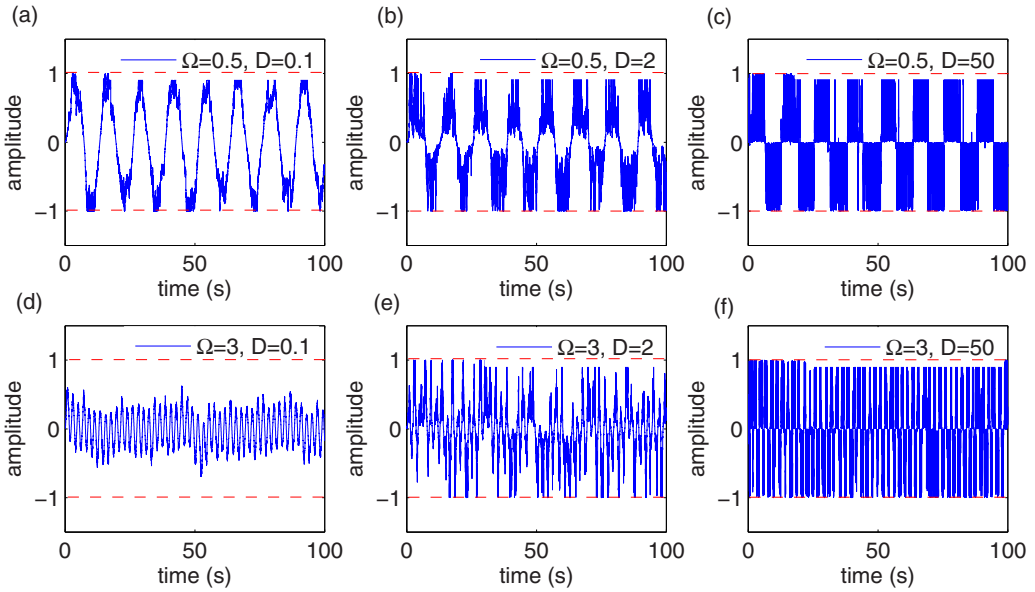

FIG. 7. Trajectories of the output response of the confined linear Langevin equation with different noise intensity D ($D = 0.1,2,50$) and different angular frequency Ω ($\Omega = 0.5,3$), at $B = 1$, $A = 1$, $a = 1$.

1. Influence of the driving angular frequency Ω on SR

The influence of the driving angular frequency Ω on the average response amplitude was first analyzed. For different values of Ω, the average response amplitude $A_{k\Omega}$ ($k = 1,3,5,7$) versus the noise intensity D is plotted in Fig. 6. The SR and *superharmonic SR* (the SRs at the superharmonics that are odd multiples of the basic driving frequency) are both found in Fig. 6. This phenomenon is different from the result shown in Refs. [4,5], which reported that in the absence of boundaries, SR will not occur in linear systems driven by multiplicative white noise because the output response is unbounded with large noise intensity D.

The resonance peak of the $A_\Omega - D$ curve is absent for a small angular frequency Ω but becomes pronounced as Ω increases. Thus, SR in the considered confined system can be easily realized with high-frequency signals. This phenomenon is different from SR in a linear system driven by multiplicative color noise and without a boundary in which SR can be easily realized with a low-frequency signal. To provide a detailed explanation, for driving frequency $\Omega = 0.5,3$, Fig. 7 presents

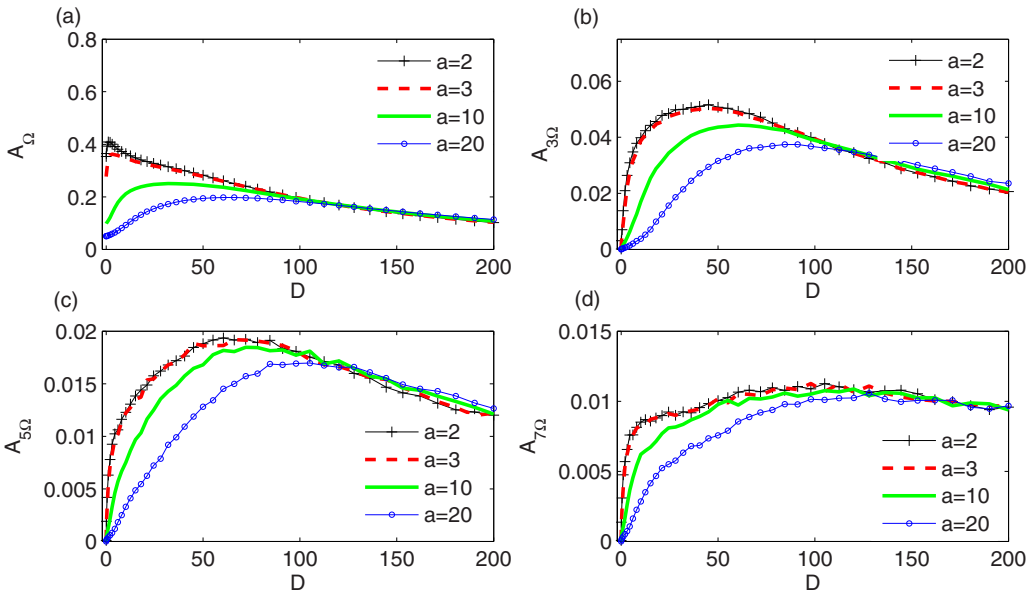

FIG. 8. Average response amplitude $A_{k\Omega}$, $k = 1,3,5,7$, versus the noise intensity D for different values of potential parameter a, with $A = 1$, $B = 1$, $\Omega = 2$. With the increase in noise intensity, each average response amplitude $A_{k\Omega}$, $k = 1,3,5,7$, increases initially and then decreases. The interwell dynamics responsible for the appearance of the main peak in $A_{k\Omega}$ is highly affected by the parameter a at smaller noise intensities but not as affected by a at high noise intensities.

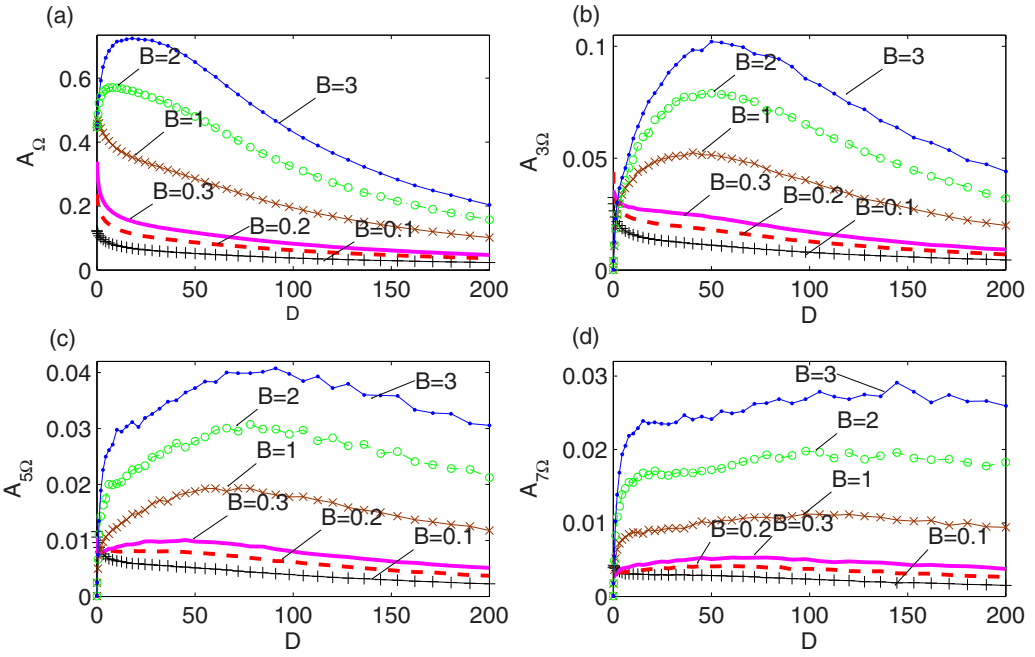

FIG. 9. Average response amplitude $A_{k\Omega}$, $k = 1,3,5,7$, versus the noise intensity D for the boundary half-width $B = 0.1,0.2,0.3,1,2,3$. For small B, e.g., $B = 0.1$, all average response amplitudes $A_{k\Omega}$ are decreasing functions of D, and no SR exists. As B increases, SR is first found in the $A_{7\Omega} - D$ curve ($B = 0.2$), second in the $A_{5\Omega} - D$ and $A_{7\Omega} - D$ curves ($B = 0.3$), third in the $A_{3\Omega} - D$, $A_{5\Omega} - D$, and $A_{7\Omega} - D$ curves ($B = 1,2$), and finally in all curves ($B = 3$).

the output trajectories of the confined Langevin equation with different values of noise intensity D. In fact, in the absence of noise (i.e., $D = 0$), the average response amplitude A_{st} is a decreasing function of the driving angular frequency Ω from Eq. (7). For large Ω [for example, $\Omega = 3$, as shown in Figs. 7(d)–7(f)], the average response amplitude A_{st} is small and far from the boundaries. The periodic drive alone is not sufficient to push the particle from one boundary to the other. However, a random disturbance with certain strength can enable the particle transition between boundaries at a random moment. In other words, in the presence of restricted boundaries, the noise and driving period may have a synergistic effect on the motion of the particle, yielding SR. With a decrease in Ω [for example, $\Omega = 0.5$, as shown in Figs. 7(a)–7(c)], the average response amplitude A_{st} increases and is closer to the boundary B. Thus, noise with low intensity is required to drive the particles to undergo transitions between the two boundaries. As a result, the position of the SR peak of D shifts

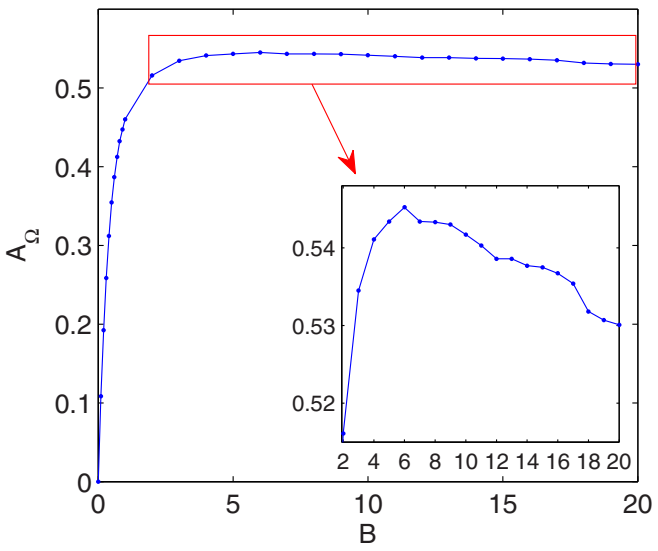

FIG. 10. Average amplitude A_Ω as a function of boundary half-width B, in which $a = 1$, $A = 1$, $D = 1$, $N = 100$, $K = 1000$, $\Omega = 2$, $h = 0.001$ s. Shows that the $A_\Omega - B$ curve has a peak for a certain value of B, and this curve represents a generalized SR.

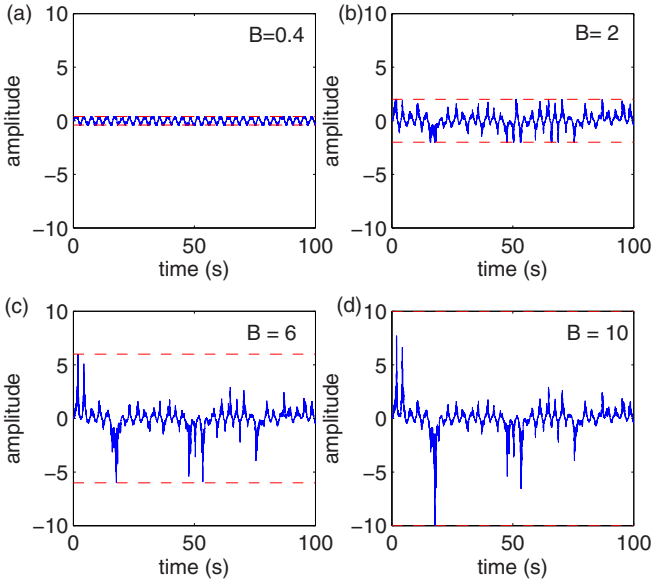

FIG. 11. Four output trajectories of the confined linear Langevin equation (1) for different values of boundaries B ($B = 0.4,2,6,10$), at $D = 1$, $A = 1$, $a = 1$.

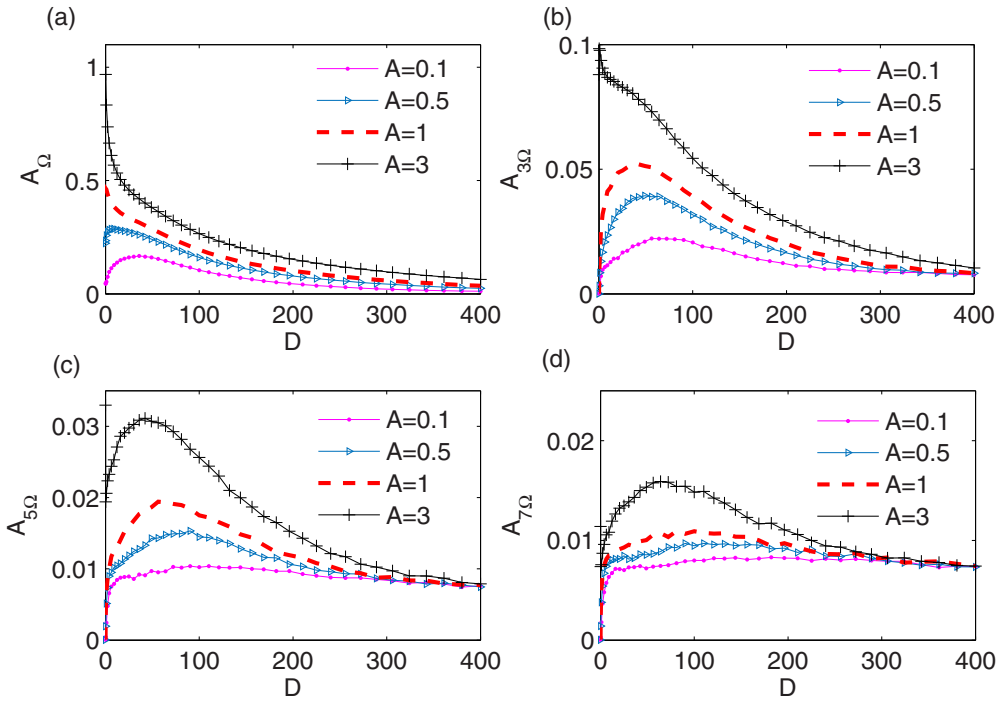

FIG. 12. Average response amplitude A_Ω as a function of noise intensity D for different values of driving amplitude A, wherein $a = 1$, $B = 1$, $\Omega = 2$, $N = 100$, $K = 1000$, and $h = 0.001$ s. The $A_\Omega - D$ curve in (a) shows that SR exists for the driving amplitude of low A (e.g., $A = 0.5$), whereas the resonance structure of the amplification disappears for the large A value (e.g., $A = 1,3$), which monotonously decreases with increasing D. Moreover, from (b)–(d), each peak values of $A_{3\Omega}$, $A_{5\Omega}$, and $A_{7\Omega}$ show a nonmonotonic behavior for increasing the modulation of driving amplitude A.

to the left. When Ω is low, the SR peak disappears and no SR occurs.

Moreover, Fig. 6 shows that the peak value of SR in the $A_{k\Omega} - D$ curve decreases as k increases, and the noise intensity, which induces the resonance at the $A_{k\Omega} - D$ curve, is an increasing function of k. Thus, the low-frequency harmonic, which is weak noise, can easily induce SR, whereas strong noise is required for the high-frequency harmonic.

2. *Influence of potential parameter a on ESR*

Figure 8 depicts how SR depends on the intrinsic frequency parameter a, for different values of a. The curves of the average amplitude $A_{k\Omega}, k = 1,3,5,7$, versus D are shown in this figure. SRs are found in all curves.

Furthermore, the peak value of the average value amplitude decreases, and the peak point shifts to high D as potential parameter a increases. The original determinist potential of the considered system $U(x) = ax^2/2$ is a classical harmonic potential, with the potential parameter a that reflects the potential strength. Therefore, as a increases, the potential well of $U(x)$ narrows. This phenomenon indicates that the height of the particle movement should be high enough to achieve the same amplitude. Consequently, strong noise energy should be applied into the system to drive the particle movement. This phenomenon is the reason for the monotonous shift in the positions of the resonance peaks to high D. Moreover, the peak value of the average value of amplitude decreases with the increase in a in Fig. 8.

3. *Influence of the boundary half-width B on SR*

Similarly, to investigate how the boundary half-width B affects the SR, for different values of B, the average amplitude $A_{k\Omega}$, $k = 1,3,5,7$, is shown versus the noise intensity D in

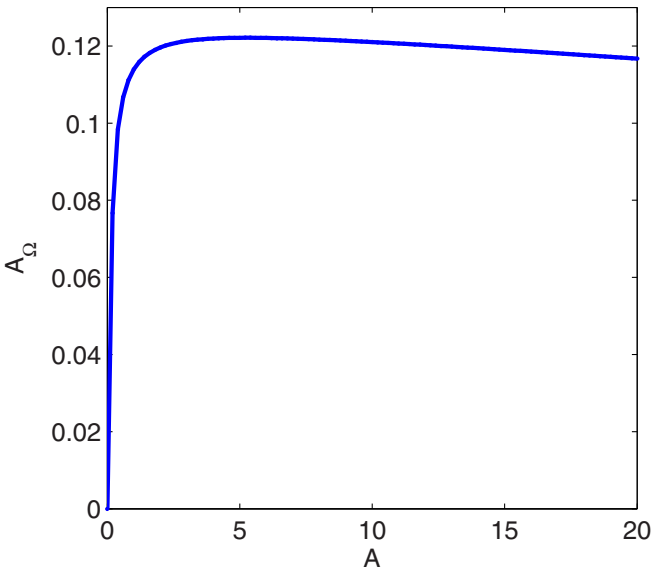

FIG. 13. Average response amplitude A_Ω as a function of driving amplitude A, wherein $a = 1$, $B = 0.1$, $\Omega = 2$, $D = 0.5$, $N = 100$, $K = 1000$, and $h = 0.001$ s.

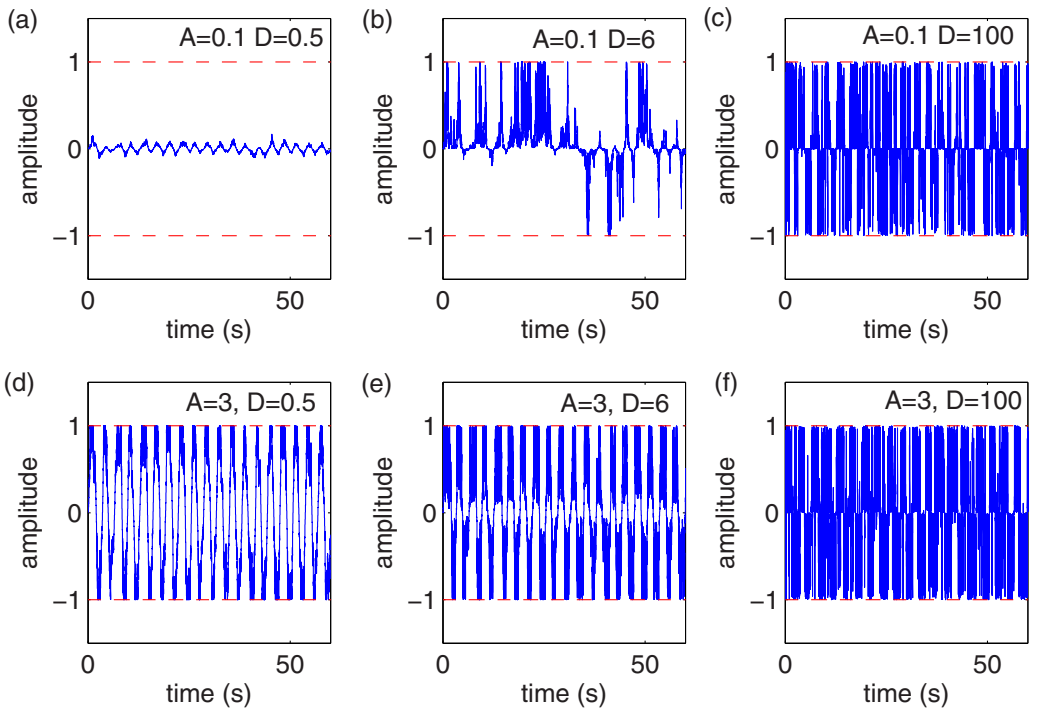

FIG. 14. For driving frequency $A = 0.1,3$, the output trajectories of the confined Langevin equation with different noise intensity D, wherein $a = 1$, $B = 1$, $\Omega = 2$, $N = 100$, $K = 1000$, and $h = 0.001$ s.

Fig. 9. The interwell dynamics responsible for the appearance of the main peak in $A_{k\Omega}$ at all the noise intensities is affected by the boundary half-width B.

With the increase in the boundary B, the SR peak of noise intensity D shifts to the right because for any given driving amplitude and large B, increased noise is required to drive the particles to undergo transitions between the two boundaries. To determine the existence of an optimized value of B exists at which the average amplitude takes its maximum value, the average amplitude A_Ω is plotted as a function of B in Fig. 10.

To provide a detailed explanation, for different values of boundaries, Fig. 11 presents four output trajectories of the confined linear Langevin equation (1). For small B [for example, $B = 0.4$, as shown in Fig. 11(a)], the average response amplitude A_{st} is larger than the boundary B. Thus, under the combined action of noise and periodic driving force, the periodic driving plays a dominant role. When B increases [for example, $B = 2,6$, as shown in Figs. 11(b) and 11(c)], the periodic drive alone is not sufficient to push the particle from one boundary to the other. A random disturbance of certain strength can enable the particle transition between boundaries, i.e., the synergistic effect between the noise and the driving period exists, thereby resulting in the gradual increase in the output amplitude. However, as the boundary further increases [for example, $B = 10$, as shown in Fig. 11(d)], the driving amplitude and noise intensity do not increase. The interaction between the periodic driving force and noise cannot easily drive the particles to undergo a transition between the two boundaries, and the average output amplitude does not increase. Finally, the output amplitude A_Ω represents a generalized SR with the increase in boundary B.

4. Influence of the driving amplitude A on SR

Finally, the dependence of SR on the driving amplitude A is considered. The average amplitude $A_{k\Omega}$, $k = 1,3,5,7$, for different values of A is shown versus the noise intensity D in Fig. 12.

Figure 13 depicts the average amplitude A_Ω as a function of driving amplitude A. Interestingly, the average amplitude A_Ω is a nonmonotonic function of driving amplitude A. The output amplitude of a linear system is always a monotonic function of the driving amplitude A. This characteristic is described by Eqs. (3) and (4), where the output amplitude A_{st} is a monotonically increasing function of A. Thus, the considered linear Langevin equation in the presence of restricted boundaries ceases to be a linear system; rather, it exhibits nonlinearity due to the boundary restrictions associated to the confinement. Therefore, a resonance also exists in the $A_\Omega - A$ curve, and a particular driving amplitude A exists for the average output amplitude A_Ω to achieve the resonance peak, which also represents another generalized SR in this study.

To provide a detailed explanation, for driving frequency $A = 0.1,3$, Fig. 14 presents trajectories of the output response of the confined Langevin equation for different values of noise intensity D. When the driving amplitude A is low [for example, $A = 0.1$, as shown in Figs. 14(a)–14(c)], the average response amplitude A_{st} is lower than the boundary half-width B. Moreover, for the low noise, the combined effect of the periodic driving force and noise cannot easily drive the particle undergo a transition between the two boundaries. When the noise increases, random perturbations with sufficient strength can enable a transition of particles between boundaries at a random moment. Therefore, the average response amplitude gradually increases because of the synergistic effect of the

noise and the periodic driving force. However, with a further increase in noise, the average response amplitude cannot easily increase because of the limitation of the boundaries. Thus, the noise begins to inhibit the effect, resulting in a decrease in the average amplitude. Thus, the conventional SR occurs. However, when the driving amplitude A increased to a certain value, the average response amplitude A_{st} became greater than boundary half-width B. The periodic driving force always plays a leading role. The average response amplitude decreases with the increase in noise. Thus, no SR occurs for the high driving force A.

IV. DISCUSSIONS AND CONCLUSIONS

In general, the dynamics of many soft condensed matter and biological systems will be affected by space limitations, which make its features notably different from the macroscopic features and thus produce peculiar effects on the systems' reaction and diffusion behavior [14–19]. The ESR, known as characteristic of small-scale and confined systems, is another nonlinear noise-induced resonant effect when a Brownian particle moves in a confined medium in the presence of a periodic driving force. Thus, it constitutes a useful mechanism for manipulation and control of single molecules and nanodevices.

In this study, the resonant response of an overdamped Langevin system driven by a periodic driving force and multiplicative white noise in the presence of constant restricted boundaries was investigated using numerical simulations. The numerical analysis of the average amplitude at both the harmonic with driving frequency Ω and the superharmonic with odd frequency $k\Omega$ ($k = 3,5,7$) showed that amplitude curves exhibit nonmonotonic behavior of the noise intensity D, i.e., SR and superharmonic SR occur. The existence of resonance peaks in the amplitude curve is the identifying characteristic of the SR phenomenon. Thus, in the considered overdamped Langevin system driven by a periodic driving force and multiplicative white noise, an increase in the spectrum amplification at an optimum value of the noise intensity D is caused by the constant geometrical restrictions. This phenomenon is different from the previous SR and ESR studies because the multiplicative color noise is a necessary condition for SR in linear systems, and an uneven boundary is a necessary condition for ESR. It is believed that the results obtained can be very helpful for further investigation of the SR phenomenon in a confined structure, and it can also open new avenues in the optimization and control of systems at the micrometer and nanometer scales, where a proper choice of the boundary and system parameters can optimize the output signal.

ACKNOWLEDGMENTS

The research was supported by the National Natural Science Foundation of China (Grants No. 11401405, No. 11501386, and No. 11501385), Science and Technology Department of Sichuan Province (Grant No. 2017JY0219) and National Natural Science Foundation of China (Grant No. 11626197).

APPENDIX: DERIVATION OF SIMULATION RECURSION FORMULA (9)

At first, we calculate the integrals in interval $[t,t+h]$ of both sides of Eq. (1) and get

$$\int_t^{t+h} \dot{x}(s)ds = -a\int_t^{t+h} x(s)ds - \int_t^{t+h} x(s)\xi(s)ds + A\int_t^{t+h} \sin(\Omega s)ds. \tag{A1}$$

Replacing $x(s)$ by $x(t)+[x(s)-x(t)]$, Eq.(A1) can be rewritten as

$$\begin{aligned} x(t+h)-x(t) &= -a\int_t^{t+h}\{x(t)+[x(s)-x(t)]\}ds - \int_t^{t+h}\{x(t)+[x(s)-x(t)]\}\xi(s)ds + A\int_t^{t+h}\sin(\Omega s)ds \\ &= -ahx(t) - a\int_t^{t+h}[x(s)-x(t)]ds - x(t)\int_t^{t+h}\xi(s)ds \\ &\quad -\int_t^{t+h}[x(s)-x(t)]\xi(s)ds - \frac{A}{\Omega}\{\cos[\Omega(t+h)]-\cos(\Omega t)\}, \end{aligned} \tag{A2}$$

where h is the integration step time.

Here, $x(s)-x(t)$ in Eq. (A2) is obtained by using Taylor expansion method at the lowest order given in Ref. [37] as follows:

$$x(s)-x(t) = [-ax(t)+A\sin(\Omega t)](s-t) - x(t)\int_t^s \xi(s_1)ds_1. \tag{A3}$$

Substituting Eq. (A3) back into the integrals in Eq. (A2) gives

$$\begin{aligned} \int_t^{t+h}[x(s)-x(t)]ds &= \int_t^{t+h}[-ax(t)+A\sin(\Omega t)](s-t)ds - x(t)\int_t^{t+h}ds\int_t^s \xi(s_1)ds_1 \\ &= \frac{1}{2}h^2[-ax(t)+A\sin(\Omega t)] - x(t)\int_t^{t+h}ds\int_t^s \xi(s_1)ds_1 \end{aligned} \tag{A4}$$

and

$$\int_t^{t+h}[x(s)-x(t)]\xi(s)ds = [-ax(t)+A\sin(\Omega t)]\int_t^{t+h}(s-t)\xi(s)ds - x(t)\int_t^{t+h}ds\int_t^s \xi(s)\xi(s_1)ds_1. \tag{A5}$$

Let

$$\Gamma_1(t+h)=\int_t^{t+h}\xi(s_1)ds_1,\ \Gamma_2(t+h)=\int_t^{t+h}ds\int_t^{s}\xi(s_1)ds_1=\int_t^{t+h}\Gamma_1(s)ds. \tag{A6}$$

Then, by using the definition of the Stratonovich integral [38] we get

$$\begin{aligned}\int_t^{t+h}(s-t)\xi(s)ds&=\int_t^{t+h}(s-t)d\Gamma_1(s)=(s-t)\Gamma_1(s)\big|_t^{t+h}-\int_t^{t+h}\Gamma_1(s)ds\\&=h\Gamma_1(t+h)-\Gamma_2(t+h)\end{aligned} \tag{A7}$$

and

$$\int_t^{t+h}\xi(s)ds\int_t^{s}\xi(s_1)ds_1=\int_t^{t+h}\xi(s)ds\,\Gamma_1(s)=\int_t^{t+h}\Gamma_1(s)d\Gamma_1(s)=\frac{1}{2}[\Gamma_1(t+h)]^2. \tag{A8}$$

Substituting Eqs. (A7) and (A8) into (A4) and (A5) gives

$$\int_t^{t+h}[x(s)-x(t)]ds=\frac{1}{2}h^2[-ax(t)+A\sin(\Omega t)]-\Gamma_2(t+h)x(t) \tag{A9}$$

and

$$\int_t^{t+h}[x(s)-x(t)]\xi(s)ds=[-ax(t)+A\sin(\Omega t)][h\Gamma_1(t+h)-\Gamma_2(t+h)]-\frac{1}{2}x(t)[\Gamma_1(t+h)]^2. \tag{A10}$$

At last, substituting of Eqs. (A9) and (A10) back into (A2) gives

$$\begin{aligned}x(t+h)-x(t)=&\left[-ah+\frac{1}{2}a^2h^2\right]x(t)-\frac{1}{2}ah^2A\sin(\Omega t)-\frac{A}{\Omega}\{\cos[\Omega(t+h)]-\cos(\Omega t)\}\\&+\left((ah-1)\Gamma_1(t+h)+\frac{1}{2}[\Gamma_1(t+h)]^2\right)x(t)-[h\Gamma_1(t+h)-\Gamma_2(t+h)]A\sin(\Omega t).\end{aligned} \tag{A11}$$

Since $\xi(s)$ is a Gaussian white noise with zero mean and variance $2D$, for any given t, $\langle\Gamma_1(t+h)\rangle=0$ and $\langle\Gamma_2(t+h)\rangle=0$. However, $\Gamma_1(t+h)$ and $\Gamma_2(t+h)$ are not independent, so we need a linear combination of two standard Gaussian random numbers δ_1,δ_2 to simulate them, from the Box-Müller formula [37] we know

$$\begin{aligned}\Gamma_1(t+h)&=\left\langle\Gamma_1^2(t+h)\right\rangle^{1/2}\delta_1,\\\Gamma_2(t+h)&=\frac{\langle\Gamma_1(t+h)\Gamma_2(t+h)\rangle}{\left\langle\Gamma_1^2(t+h)\right\rangle^{1/2}}\delta_1+\left[\left\langle\Gamma_2^2(t+h)\right\rangle-\frac{\langle\Gamma_1(t+h)\Gamma_2(t+h)\rangle^2}{\left\langle\Gamma_1^2(t+h)\right\rangle}\right]^{1/2}\delta_2,\end{aligned} \tag{A12}$$

where the variance and the cross correlation of $\Gamma_1(t+h)$ and $\Gamma_2(t+h)$ are readily determined from their definition. Since $B(t+h)=\int_t^{t+h}\xi(s)ds\sim N(0,2Dh)$, thus, we have

$$\Gamma_1(t+h)=B(t+h),\ \Gamma_2(t+h)=\int_t^{t+h}B(s)ds. \tag{A13}$$

Moreover, $\langle B(s_1)B(s_2)\rangle=2D\min(s_1,s_2)$, thus,

$$\left\langle\Gamma_1^2(t+h)\right\rangle=2Dh, \tag{A14}$$

$$\left\langle\Gamma_2^2(t+h)\right\rangle=\int_t^{t+h}\int_t^{t+h}\langle B(s_1)B(s_2)\rangle ds_1ds_2=\frac{2}{3}Dh^3, \tag{A15}$$

$$\begin{aligned}\langle\Gamma_1(t+h)\Gamma_2(t+h)\rangle&=\left\langle[B(t+h)-B(t)]\int_t^{t+h}B(s)ds\right\rangle\\&=\int_t^{t+h}\langle B(t+h)B(s)\rangle ds-\int_t^{t+h}\langle B(t)B(s)\rangle ds=Dh^2.\end{aligned} \tag{A16}$$

Therefore, after calculations we get

$$\Gamma_1(t+h)=\sqrt{2Dh}\delta_1,\ \Gamma_2(t+h)=\frac{1}{2}\sqrt{2Dh}h\delta_1+\frac{1}{2\sqrt{3}}\sqrt{2Dh}h\delta_2, \tag{A17}$$

where δ_1,δ_2 are Gaussian distributed random numbers with zero mean and unit variance.

[1] S. Fauve and F. Heslot, Phys. Lett. A **97**, 5 (1983).
[2] Y. Jia, S. N. Yu, and J. R. Li, Phys. Rev. E **62**, 1869 (2000).
[3] M. E. Inchiosa and A. R. Bulsara, Phys. Rev. E **53**, 2021 (1996).
[4] A. Fulinski, Phys. Rev. E **52**, 4523 (1995).
[5] V. Berdichevsky and M. Gitterman, Europhys. Lett. **36**, 161 (1996).
[6] V. Berdichevsky and M. Gitterman, Phys. Rev. E **60**, 1494 (1999).
[7] L. Zhang, S. C. Zhong, H. Peng, and M. K. Luo, Chin. Phys. Lett. **28**, 090505 (2011).
[8] S. C. Zhong, H. Ma, H. Peng, and L. Zhang, Nonlin. Dyn. **82**, 535 (2015).
[9] A. Longtin, J. Stat. Phys. **70**, 309 (1993).
[10] S. M. Begrukov and I. Vodyanoy, Nature (London) **385**, 319 (1997).
[11] R. Castro and T. Sauer, Phys. Rev. Lett. **79**, 1030 (1997).
[12] Q. Y. Wang, M. Perc, Z. Duan, and G. Chen, Chaos **19**, 023112 (2009).
[13] C. B. Gan, M. Perc, and Q. Y. Wang, Chin. Phys. B **19**, 040508 (2010).
[14] I. Goychuk, P. Hänggi, J. L. Vega, and S. Miret-Artés, Phys. Rev. E **71**, 061906 (2005).
[15] F. Guo and S. F. Li, J. Korean Phys. Soc. **60**, 327 (2012).
[16] B. Hille, *Ion Channels of Excitable Membranes* (Sinauer Associates, Sunderland, UK, 2001).
[17] L. Liu, P. Li, and S. A. Asher, Nature (London) **397**, 141 (1999).
[18] A. M. Berezhkovskii and S. M. Bezrukov, Biophys. J. **88**, L17 (2005).
[19] D. Reguera and J. M. Rubí, Phys. Rev. E **64**, 061106 (2001).
[20] A. Schüring, S. M. Auerbach, S. Fritzsche, and R. Haberlandt, J. Chem. Phys. **116**, 10890 (2002).
[21] K. S. Schweizer and E. J. Saltzman, J. Chem. Phys. **119**, 1181 (2003).
[22] D. Reguera, G. Schmid, P. S. Burada, J. M. Rubí, P. Reimann, and P. Hänggi, Phys. Rev. Lett. **96**, 130603 (2006).
[23] P. S. Burada, G. Schmid, D. Reguera, J. M. Rubí, and P. Hänggi, Europhys. Lett. **87**, 50003 (2009).
[24] N. Shi and V. M. Ugaz, Phys. Rev. E **89**, 012138 (2014).
[25] H. Ding, H. Jiang, and Z. Hou, J. Chem. Phys. **142**, 194109 (2015).
[26] Z. Liu, L. Du, W. Guo, and D. C. Mei, Eur. Phys. J. B **89**, 222 (2016).
[27] P. K. Ghosh, F. Marchesoni, S. E. Savel'ev, and F. Nori, Phys. Rev. Lett. **104**, 020601 (2010).
[28] S. Sinha and B. K. Chakrabarti, Phys. Rev. E **58**, 8009 (1998).
[29] S. Sinha, Phys. A (Amsterdam) **270**, 204 (1999).
[30] V. Strelkov, Phys. Rev. Lett. **104**, 123901 (2010).
[31] J. H. Yang, M. A. F. Sanjuán, H. G. Liu, and H. Zhu, Nonlin. Dyn. **87**, 1721 (2017).
[32] R. A. Ganeev, J. Zheng, M. Wöstmann, H. Witte, P. V. Redkin, and H. Zacharias, Eur. Phys. J. D **68**, 325 (2014).
[33] S. R. Nielsen and M. T. Sichani, Probab. Eng. Mech. **26**, 44 (2011).
[34] P. V. Redkin and R. A. Ganeev, Phys. Rev. A **81**, 063825 (2010).
[35] L. C. Evans, *An Introduction to Stochastic Differential Equations* (American Mathematical Society, Providence, RI, 2014).
[36] E. Platen, Acta Numer. **8**, 197 (1999).
[37] J. D. Bao, Y. Z. Zhuo, and X. Z. Wu, J. Stat. Phys. **66**, 1653 (1992).
[38] I. Karatzas and S. E. Shreve, *Brownian Motion and Stochastic Calculus* (Springer, New York, 1991).